Indian Journal of Pure & Applied Physics
Vol. 60, February 2022, pp. 150-156

A Dielectrically Modulated AlGaN/InN/GaN Nanoelectronic High Electron Mobility Transistor based Biosensor for Protein Detection

Sanjib Kalita* & Kethepalli Mallikarjuna

Department of Electronics and Communication Engineering, Rajeev Gandhi Memorial College of Engineering and Technology, Nandyal, Kurnool, Andhra Pradesh 518 501, India

Received 4 September 2021; accepted 14 January 2022

In this work, a high electron mobility transistor (HEMT) based biosensor is designed to detect the virus-protein. Conduction band engineering of the biosensor is studied. DC and RF properties of the designed biosensor are studied. Sensitivity of the biosensor is studied corresponding to electric field, surface potential, drain current, transconductance, and current gain cut-off frequency. Sufficient sensitivity is obtained corresponding to each electrical parameter to detect the virus-protein. This work may be helpful to design and experimentally fabricate the HEMT based biosensor.

Keywords: Protein, Dielectric constant, Transconductance, Sensitivity, Drain current.

1 Introduction

Vu and Chen have reviewed on the field effect transistor biosensors (Bio-FET) towards the biomedical applications including the evolution of nano-transducers for FET-based sensors[1]. Sarangadharan et al have reviewed on the performance of high field modulated FET biosensors including the characteristics of high field gated FET biosensor[2]. Also, a rapid extracellular vesicle (EV) quantification methodology is realised using a high field modulated AlGaN/GaN HEMT biosensor[3]. Recently, a dielectric modulated double-gate tunnel field-effect transistor (DG-TFET) based biosensor is presented by analytical treatments and simulation results showing advantages with respect to earlier biosensors[4].

High electron mobility transistor (HEMT) may become a suitable component to design the biosensor for detection of virus-protein[5-8]. The detection of membrane protein is a suitable technique to identify the virus in test solution. For this purpose, it is important to analyse the electrical performance of any designed HEMT based biosensor in terms of DC and RF characteristics[9-13]. Many authors have recently reported the physics based analytical models for electrical characteristics of HEMTs[14-18].

Also, theoretical and experimental investigations on characteristics of different HEMT structures are already reported[19-25]. Different properties of device materials have significant influences on the electrical characteristics of HEMTs[26-31]. These earlier investigations may be helpful to design the HEMT based biosensor to detect any virus-protein. The dielectric constant of virus-protein varies between 2 to 4 according to available literatures[5, 32]. Dielectric constant of virus-protein may play an important role in the detection by any designed HEMT based biosensor.

In this work, a HEMT based biosensor is designed to detect the virus-protein using the test solution. Static and transfer characteristics of designed biosensor are individually investigated. Variations in transconductance and current gain cut-off frequency with gate voltage are also individually investigated. Variations in electric field and surface potential with respect to the lateral length of device are also individually investigated. Sensitivities of designed biosensor corresponding to the electric field, surface potential, drain current, transconductance, and current gain cut-off frequency are individually investigated. This work may be suitable to experimentally fabricate the HEMT based biosensor in future.

2 Description of Model in Simulation

In this work, all the simulations are carried out in the SILVACO-ATLAS physical simulator using the following models: Shockley Read Hall (SRH), band gap narrowing, Auger recombination, and Fermi Dirac statistics. Newton trap numerical solver is used in the device simulation. Fig. 1 shows the simulated

*Corresponding author: (E-mail: sanjib.kalita25@gmail.com)

structure of proposed HEMT based biosensor to detect the virus-protein. Device dimensions are clearly shown in Fig. 1. Source has the lateral length of 200 nm. Drain has the lateral length of 200 nm. Source to gate distance is 200 nm, and gate to drain distance is 600 nm. Both of source and drain have equal height as 50 nm. AlGaN thickness is 10 nm.

InN thickness is 0.36 nm. The atomic layer of InN is inserted between AlGaN and GaN to achieve higher drain current resulting into the larger sensitivity of designed biosensor[33]. GaN thickness is 81 nm. The gate and cavity dimensions are clearly shown in Fig. 1. The cavity starts laterally from 700 nm after the left most edge of simulated structure. Any test solution should be placed in the cavity to determine the corresponding sensitivity of the biosensor. Total lateral length of the simulated device is 1500 nm. In the whole simulation work, the range of dielectric constant (K) of virus-protein is considered as 2 to 4[5, 32]. Air (K=1) is considered as reference dielectric in the simulation.

Till now, many research groups tried to optimize the AlGaN/GaN HEMT device for maximum performance. In this work, we have optimized AlGaN/InN/GaN HEMT and obtained the maximum DC and RF performances at a fixed dimension of 10 nm and 0.36 nm of AlGaN and InN respectively. Due to the insertion of InN layer between the AlGaN and GaN layers, the mobility is increased and the high-frequency performance is improved[34]. According to available literature, the atomic layer of InN above GaN layer produces high quality HEMT device since it reduces the defects due to lattice mismatch between the layers[35]. Already many researchers have deposited atomic layers of different thickness using the plasma enhanced atomic layer deposition (PE-ALD) technique. The growth per cycle (GPC) for AlN is 0.6 Å/cycle and that for InN is 0.36 Å/cycle[36-38]. In this present simulation, 3.6 Å *i.e.* 0.36 nm is considered for AlN layer and for InN layer which can be grown above the GaN layer by depositing 6 cycles and 10 cycles for AlN and InN respectively using PE-ALD technique.

In addition to dielectric constant, various parameters are available to detect the proteins, for example, surface charge, electrolyte ionic strength, and antibody-antigen interactions[39]. We have studied the sensitivity of biosensor by considering only dielectric constant of protein biomolecules since sharp variation in dielectric constant of different protein biomolecules shows a good change in electrical behaviour of designed biosensor[40].

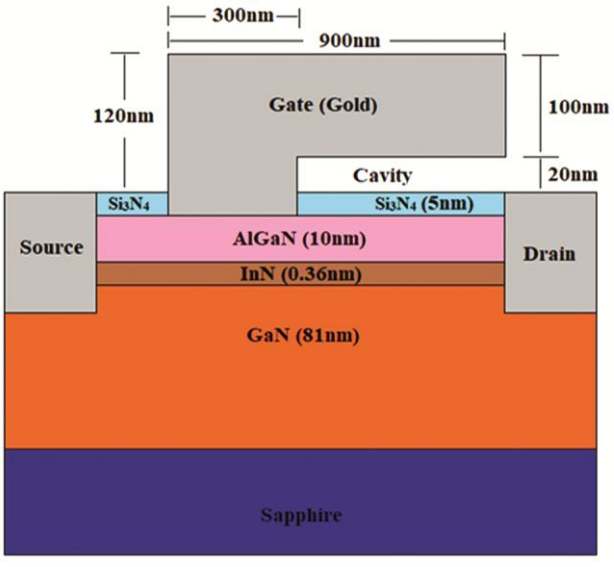

Fig. 1 — Structure of the proposed HEMT based biosensor to detect the virus-protein.

3 Results and Discussion

3.1 Calibration of proposed biosensor

Our work is completely based on simulation studies of a proposed HEMT based bio-sensor. In the simulation, we have calibrated the designed HEMT as per one available literature by introducing same dimensions, biasing conditions and doping concentration[41]. Approximately similar DC characteristics are achieved with respect to that literature as shown in Fig. 2.

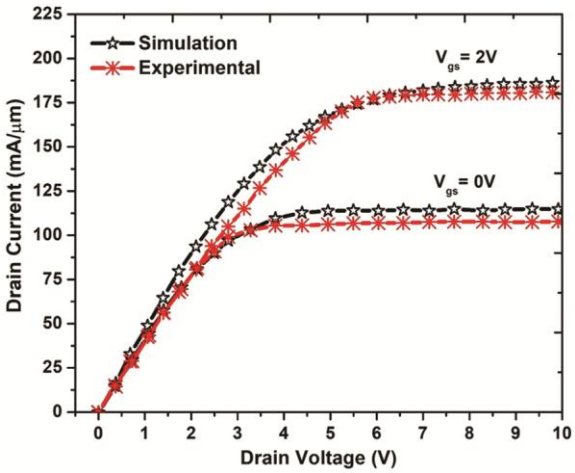

Fig. 2 — Variation of drain current with drain voltage is shown to calibrate the designed device as per one available literature. Prominent similarity among simulation curves and already published experimental curves are observed.

3.2 DC and RF performance of HEMT based biosensor

Figure 3 shows the formation of quantum well in the layer of InN at the heterojunction generating the two-dimensional electron gas (2DEG). Due to the large band gap of InN layer, increased conduction band discontinuity is observed at the junction of InN and GaN layer which generates the quantum well. All the electrons of nearby layers are confined at this quantum well to form 2DEG[14-19]. Fig. 4 shows the static drain characteristics of proposed HEMT based biosensor corresponding to the air dielectric (K=1). Air (K=1) corresponds to the reference dielectric. For air dielectric, the drain current is higher at higher drain voltage corresponding to any particular gate voltage[9]. Similar static drain characteristics are observed for virus-protein dielectrics having the range of dielectric constant from 2 to 4[9].

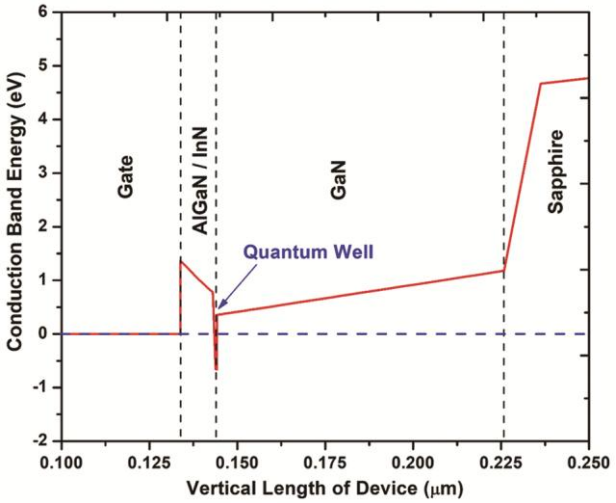

Fig. 3 — Formation of quantum well at heterojunction is shown in the proposed HEMT based biosensor.

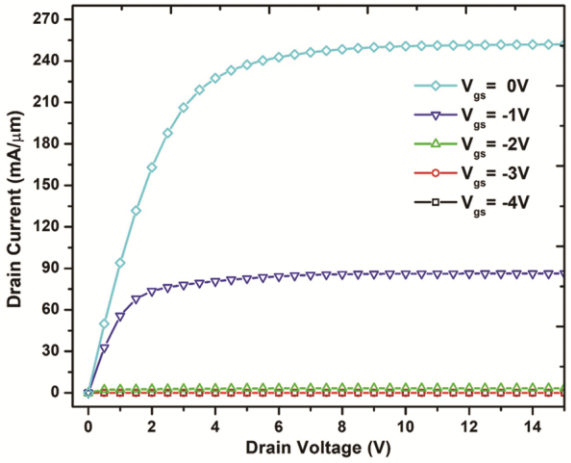

Fig. 4 — Static drain characteristics of the proposed HEMT based biosensor is shown for air dielectric (K=1).

Figure 5 shows the transfer characteristics of the proposed HEMT based biosensor. The drain current is higher at higher gate voltage corresponding to any particular dielectric constant of test solution[9]. The drain current is higher corresponding to larger dielectric constant at any particular gate voltage[9]. Fig. 6 shows the variation in transconductance with gate voltage corresponding to different dielectric constants. The transconductance is found to be higher at larger dielectric constant.

The formula to calculate the current gain cut-off frequency is shown as follows:

$$f_T = \frac{g_m}{2\pi(C_{gs}+C_{gd})} \quad \ldots (1)$$

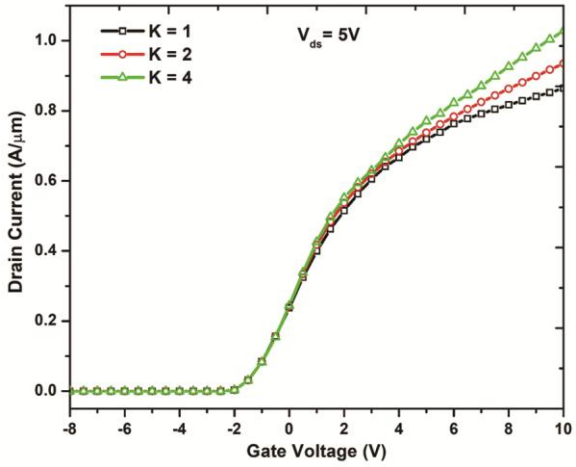

Fig. 5 — Transfer characteristics of the proposed HEMT based biosensor are shown. Air (K=1) corresponds to the reference dielectric.

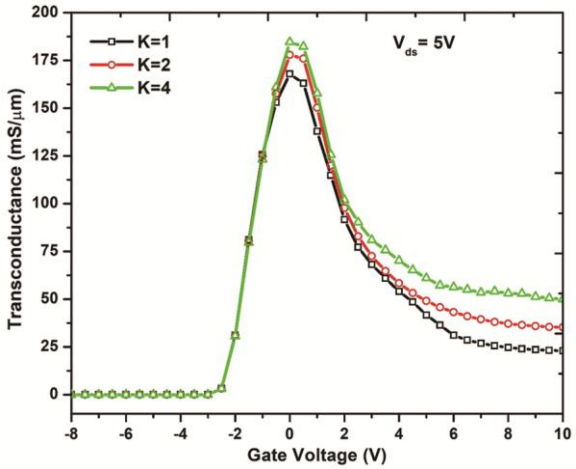

Fig. 6 — Variation in transconductance with gate voltage is shown at different dielectric constants corresponding to the selected test solutions. Air (K=1) corresponds to the reference dielectric.

'gm', 'Cgs' and 'Cgd' are the transconductance, gate to source capacitance, and gate to drain capacitance respectively. Fig. 7 shows the variation in current gain cut-off frequency with gate voltage corresponding to different dielectric constants. The current gain cut-off frequency is higher at larger dielectric constant.

Figure 8 shows the variation in electric field with lateral length of device corresponding to each dielectric constant. Inside the cavity, the electric field is higher corresponding to larger dielectric constant. Fig. 9 shows the variation in surface potential with lateral length of device corresponding to each dielectric constant. Inside the cavity, the surface potential is higher corresponding to larger dielectric constant.

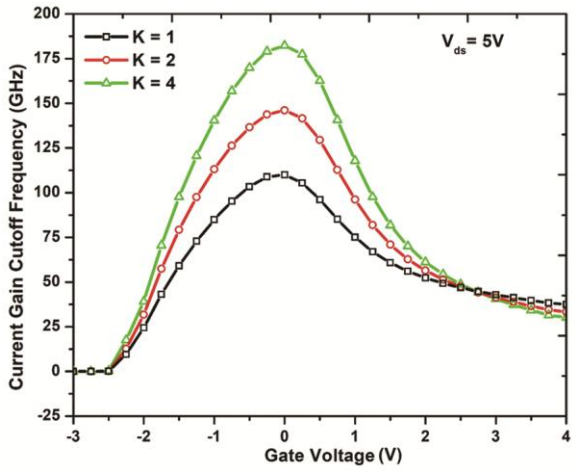

Fig. 7 — Variation in current gain cut-off frequency with gate voltage is shown at different dielectric constants corresponding to the selected test solutions.

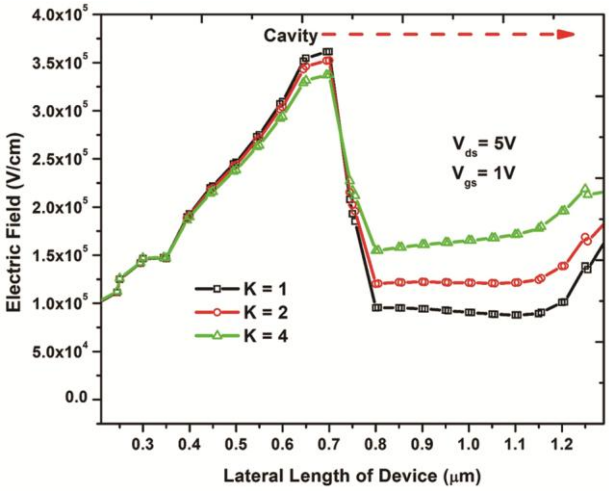

Fig. 8 — Variation in electric field with lateral length of device is shown at different dielectric constants corresponding to the selected test solutions.

3.3 Analysis on Sensitivity of the designed biosensor

The formula to calculate the percentage sensitivity is shown as follows:

$$\%\ Sensitivity = \left|\frac{Q_1 - Q_2}{Q_1}\right| \times 100 \quad \ldots (2)$$

Q1 is the value of quantity when the cavity is filled with air (K=1). Q2 is the value of quantity when the cavity is filled with virus-protein. Q1 and Q2 correspond to the values of any electrical parameter under consideration. The electrical parameters to calculate the percentage sensitivity are electric field, surface potential, drain current, transconductance, and current gain cut-off frequency.

Figures 10 to 14 show the sensitivity values for the range of dielectric constant values (K=2 to 4)

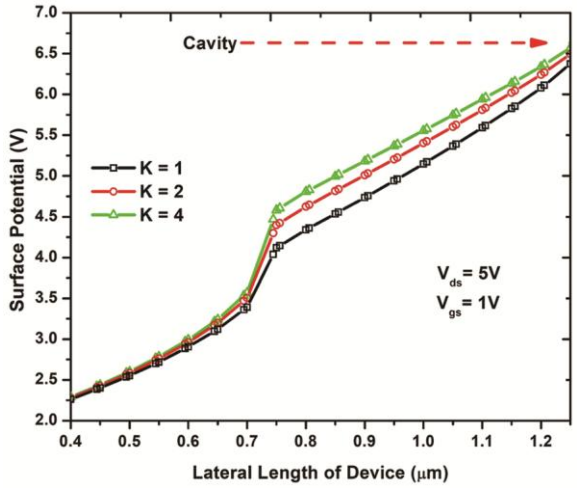

Fig. 9 — Variation in surface potential with lateral length of device is shown at different dielectric constants corresponding to the selected test solutions.

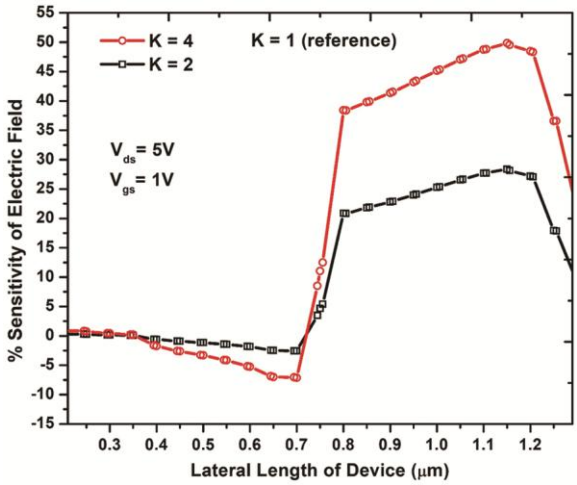

Fig. 10 — Variation in sensitivity of electric field with lateral length of device is shown at different dielectric constants corresponding to the selected test solutions.

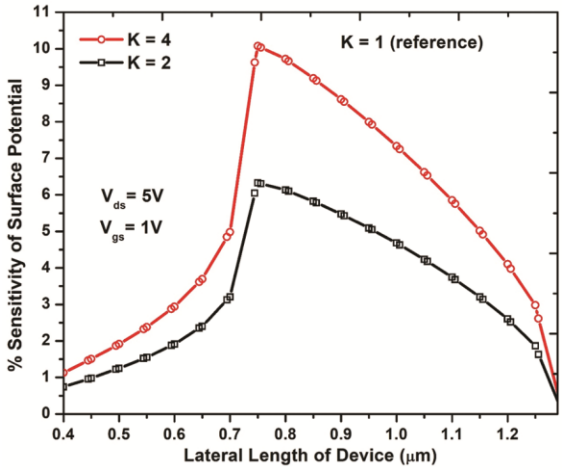

Fig. 11 — Variation in sensitivity of surface potential with lateral length of device is shown at different dielectric constants corresponding to the selected test solutions.

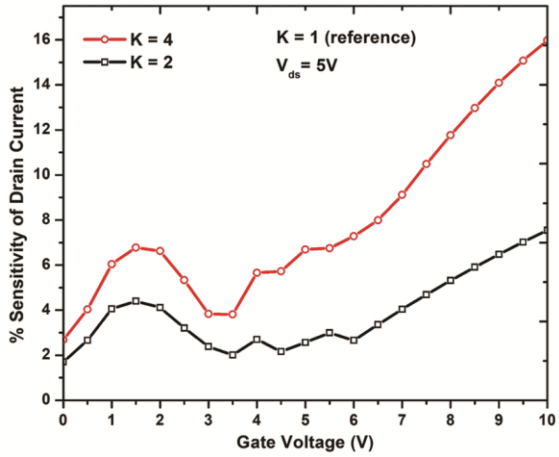

Fig. 12 — Variation in sensitivity of drain current with gate voltage is shown at different dielectric constants corresponding to the selected test solutions.

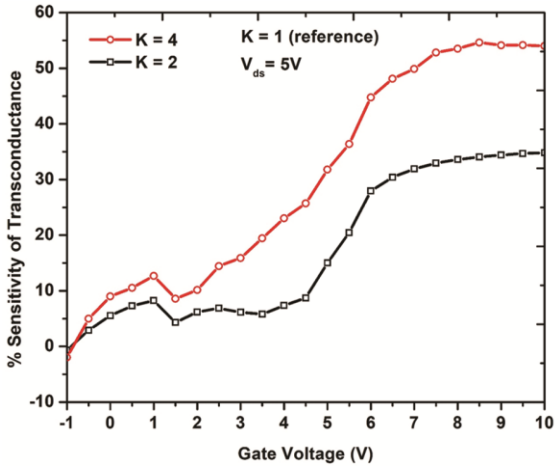

Fig. 13 — Variation in sensitivity of transconductance with gate voltage is shown at different dielectric constants corresponding to the selected test solutions.

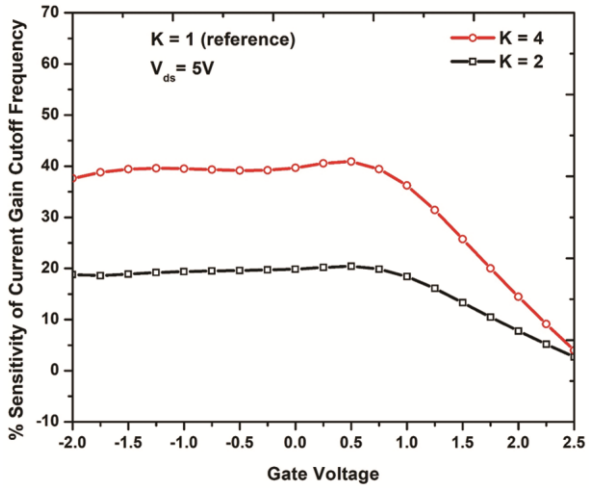

Fig. 14 — Variation in sensitivity of current gain cut-off frequency with gate voltage is shown at different dielectric constants corresponding to the selected test solutions.

corresponding to virus-protein with respect to the considered electrical parameters. According to Fig. 10, sensitivity of electric field is higher corresponding to larger dielectric constant below the cavity. According to Fig. 11, sensitivity of surface potential is higher for larger dielectric constant below the cavity. In Fig. 12, sensitivity of drain current is higher for larger dielectric constant with respect to gate voltage. In Fig. 13, sensitivity of transconductance is higher for larger dielectric constant with respect to gate voltage. In Fig. 14, sensitivity of current gain cut-off frequency is higher for larger dielectric constant with respect to gate voltage. Certain range of values of sensitivity is found corresponding to virus-protein with respect to each electrical parameter. Therefore, it is easy to detect the virus protein according to the value of sensitivity determined by the designed biosensor.

The sensitivity of biosensors can be done in wet (solution) of dry (air) environment[42]. Due to the high dielectric constant of water (K=80), the sensitivity is considerably reduced in the wet environment, as compared to the lower dielectric constant of biomolecules[40-44]. In this work, we have proposed a dielectric modulated HEMT based protein biosensor and studied the characteristics using SILVACO-ATLAS physical simulator in dry environment. During these studies, we have considered fully filled cavity with biomolecules. As, the fully filled cavity is rarely encountered, we have also studied the drain current sensitivity of the proposed biosensor in different possible cases of partially filled cavities.

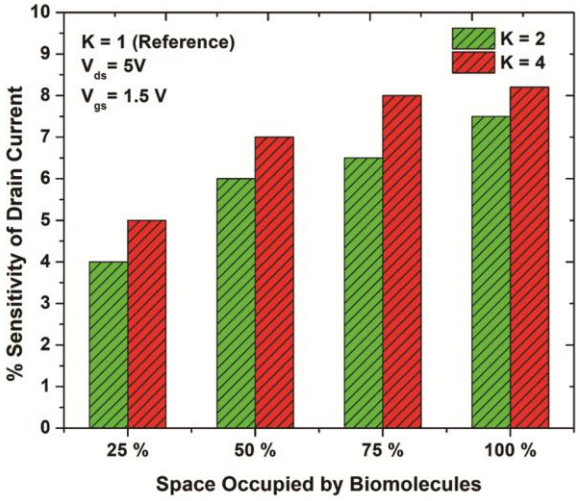

Fig. 15 — Variation in percentage sensitivity of drain current with respect to space occupied by biomolecules is shown.

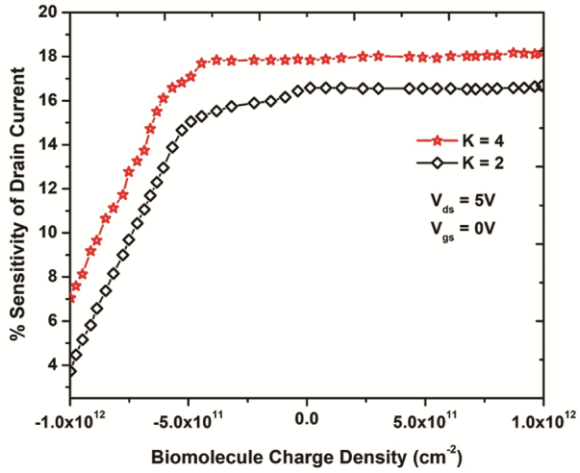

Fig. 16 — Variation in percentage sensitivity of drain current with respect to biomolecule charge density is shown.

Fig. 15 shows the percentage drain current sensitivity of the biosensor in different percentage of space occupied by the biomolecules inside the cavity at dielectric constant (K) of 2 and 4 respectively. Again, the sensitivity of the dielectric modulated biosensors can be affected by bimolecular charge, as most of the biomolecules have a net electrostatic charge. So, we have also studied the effect of bimolecular charge on the drain current sensitivity of dielectric modulated HEMT based biosensor. Fig. 16 shows the variation of percentage sensitivity of drain current at different biomolecule charge density.

To study the sensing kinetics, we have to observe the biosensor in wet environment after fabrication. Hence, this is our one future research work to fabricate and study the biosensor in wet environment.

4 Conclusions

Drain current of designed biosensor increases with drain voltage at any particular gate voltage corresponding to the test dielectric solution due to the formation of quantum well at heterojunction generating the 2DEG. Drain current of biosensor increases with gate voltage in transfer characteristics. In our study, higher drain current corresponds to larger dielectric constant. Transconductance of biosensor is higher corresponding to larger dielectric constant. Current gain cut-off frequency is higher corresponding to larger dielectric constant. Electric field is higher in the cavity corresponding to the test solution of larger dielectric constant. Surface potential is higher inside the cavity corresponding to the test solution of larger dielectric constant. Sensitivities of electric field, surface potential, drain current, transconductance and current gain cut-off frequency are individually higher inside the cavity corresponding to the test solution of larger dielectric constant. This work may be helpful to design and experimentally fabricate the HEMT based biosensor to detect the virus-protein.

References

1 Vu C A & Chen W Y, *Sensors*, 19 (2019) 4214.
2 Sarangadharan I, Pulikkathodi A K, Chu C H, Chen Y W, Regmi A, Chen P C, Hsu C P & Wang Y L, *ECS J Solid State Sci Technol*, 7 (2018) Q3032.
3 Pulikkathodi A K, Sarangadharan I, Lo C Y, Chen P H, Chen C C & Wang Y L, *Int J Mol Sci*, 19 (2018) 2213.
4 Narang R, Saxena M, Gupta R S & Gupta M, *IEEE Electron Dev Lett*, 33 (2012) 266.
5 Parihar M S & Kranti A, *Nanotechnology*, 26 (2015) 1.
6 Im H, Huang X J, Gu B & Choi Y K, *Nature Nanotechnol*, 2 (2007) 430.
7 Lahgere A, Sahu C & Singh J, *Electron Lett*, 51 (2015) 1284.
8 Yadav S, Madhukar R, Sharma D, Aslam M, Soni D & Sharma N, *Appl Phys A*, 124 (2018) 517.
9 Charfeddine M, Belmabrouk H, Zaidi M A & Maaref H, *J Mod Phys*, 3 (2012) 881.
10 Chattopadhyay M K & Tokekar S, *Microelectron J*, 39 (2008) 1181.
11 Chattopadhyay M K & Tokekar S, *Solid-State Electron*, 50 (2005) 220.
12 Chattopadhyay M K & Tokekar S, *Microwave Opt Technol Lett*, 49 (2006) 382.
13 Korwal M, Haldar S, Gupta M & Gupta R S, *Microwave Opt Technol Lett*, 38 (2003) 371.
14 Khandelwal S, Goyal N & Fjeldly T A, *IEEE Trans Electron Dev*, 58 (2011) 3622.
15 Khandelwal S, Chauhan Y S & Fjeldly T A, *IEEE Trans Electron Dev*, 59 (2012) 2856.
16 Khandelwal S, Yadav C, Agnihotri S, Chauhan Y S, Curutchet A, Zimmer T, Jaeger J C D, Defrance N & Fjeldly T A, *IEEE Trans Electron Dev*, 60 (2013) 3216.

17 Khandelwal S & Fjeldly T A, *Solid-State Electron*, 76 (2012) 60.
18 Khandelwal S, Goyal N & Fjeldly T A, *Solid-State Electron*, 79 (2013) 22.
19 Kalita S & Mukhopadhyay S, *J Nanoelectron Optoelectron*, 13 (2018) 1123.
20 Mishra U K, Parikh P & Wu Y F, *Proc IEEE*, 90 (2002) 1022.
21 Mishra U K, Shen L, Kazior T E & Wu Y F, *Proc IEEE*, 96 (2008) 287.
22 Frayssinet E, Knap W, Lorenzini P, Grandjean N, Massies J, Skierbiszewski C & T Suski, *Appl Phys Lett*, 77 (2000) 2551.
23 Visalli D, Hove M V, Derluyn J, Degroote S, Leys M, Cheng K, Germain M & G Borghs, *Jpn J Appl Phys*, 48 (2009) 04C101.
24 Kuzuhara M & Tokuda H, *IEEE Trans Electron Dev*, 62 (2015) 405.
25 Kuzmik J, *IEEE Electron Dev Lett*, 22 (2001) 510.
26 Shrestha N M, Li Y & Chang E Y, *Jpn J Appl Phys*, 53 (2014) 04EF08.
27 Teke A, Gokden S, Tulek R, Leach J H, Q Fan, Xie J, Ozgur U, Morkoc H, Lisesivdin S B & Ozbay E, *New J Phys*, 11 (2009) 063031.
28 Morko C H, Cingolani R & Gil B, *Solid-State Electron*, 43 (1999) 1909.
29 Ambacher O, Smart J, Shealy J R, Weimann N G, Chu K, Murphy M, Schaff W J, Eastman L F, Dimitrov R & Wittmer L, *J Appl Phys*, 87 (1999) 3222.
30 Ambacher O, Majewski J, Miskys C, Link A, Hermann M, Eickhoff M, Stutzmann M, Bernardini F, Fiorentini V & Tilak V, *J Phys Condens Matter*, 14 (2002) 3399.
31 Pela R R, Caetano C, Ferreira L G, Furthmuller J & Teles L K, *Appl Phys Lett*, 98 (2011) 151907.
32 Gilson M K & Honig B H, *Biopolymers*, 25 (1986) 2097.
33 Miao M S & Walle C G V D, *Appl Phys Exp*, 8 (2015) 024302.
34 Lenka T R & Panda A K, *Semiconductors*, 45 (2011) 1211.
35 Yoshikawa A, Che S B, Yamaguchi W, Saito H, Wang X Q, Ishitani Y & Hwang E S, *Appl Phys Lett*, 90 (2007) 073101.
36 Legallais M, Mehdi H, David S, Bassani F, Labau S, Pelissier B, Baron T, Martinez E, Ghibaudo G & Salem B, *ACS Appl Mater Interf*, 12 (2020) 39870.
37 Rontu V, Sippola P, Broas M, Ross G, Sajavaara T, Lipsanen H, Paulasto-Krockel M, S Franssila, *J Vac Sci Technol A*, 36 (2018) 021508.
38 Deminskyi P, Rouf P, Ivanov I G, Pedersen H, *J Vac Sci Technol A*, 37 (2019) 020926.
39 Hemaja V & Panda D K, *Silicon*, (2021) doi: 10.1007/s12633-020-00937-w.
40 Kannan N, Kalra S, Kumar M J, *IEEE Sensors Lett*, 1 (2017) 4500904.
41 Hu W D, Chen X S, Quan Z J, Zhang X M, Huang Y, Xia C S, Lu W & Ye P D, *J Appl Phys*, 102 (2007) 034502.
42 Kim J Y, Ahn J H, Choi S J, Im M, Kim S, Duarte J P, Kim C H, Park T J, Lee S Y & Choi Y K, *IEEE Trans Nanotechnol*, 11 (2012) 390.
43 Ahmad M A, Milhem R M, Panicker N G, Rizvi T A & Mustafa F, *Sci Rep*, 6 (2016) 29089.
44 Mehrotra P, Chatterjee B & Sen S, *Sensors*, 19 (2019) 1013.